



Hypervelocity Impact Testing of Transparent Spacecraft Materials

Richard R. Burt*, Eric L. Christiansen**

*The Boeing Company, Mail Code HM5-20, 13100 Space Center Blvd., Houston, TX 77059

**NASA Johnson Space Center, Mail Code SX2, Houston, TX 77058

Abstract

Transparent materials have been used by NASA as windows since the beginning of the Human Space Flight Program. This paper provides results of an intensive effort to determine hypervelocity impact characteristics and develop damage equations for transparent materials currently used on the International Space Station and Space Shuttle programs. The materials considered here are fused silica glass, tempered glass, and polycarbonate. Hypervelocity impact tests on these materials under a variety of impact conditions are described. Penetration equations are defined that allow assessment of impact damage to windows and are useful in BUMPER code meteoroid/orbital debris (M/OD) assessments.

© 2003 Published by Elsevier Ltd.

Keywords: shielding, meteoroid/orbital debris, penetration equations, glass, fused-silica, polycarbonate

Notation

D	front side spall/crater diameter (cm)
d_c	critical projectile diameter (cm) of failure threshold
d_p	projectile diameter (cm)
KE_f	critical projectile kinetic energy (J)
KE_n	normal component of projectile kinetic energy (J) = $KE \cos\theta$
KE_{spall}	projectile kinetic energy above which back side spallation occurs (J)
P	crater depth (cm)
ρ_p	projectile density (g/cm^3)
θ	impact angle from surface normal (deg)
t	materials thickness (cm)
V	projectile velocity (km/s)
V_n	normal component of velocity (km/s) = $V \cos\theta$

1. Introduction

Since the beginning of space flight, orbital vehicles have used windows for means of guidance and navigation, photography, observation and monitoring of external surfaces and extravehicular activity (EVA). Primarily fused silica (SiO_2) windows have been used because of its optical clarity and its stability in the space environment. With the assembly of the International Space Station (ISS) currently underway in orbit, NASA is using advances in material technology to enhance the capabilities of the new orbiting research facility. The NASA Johnson Space Center Hypervelocity Impact Technology Facility (HITF) [1] has been testing hypervelocity impact performance of several window and

transparent window cover materials currently on the Space Shuttle and ISS. The results of the testing have been used to develop penetration and damage equations for these materials that are then programmed in BUMPER code for micrometeoroid/orbital debris (M/OD) assessments [2-4].

Windows constitute a small percentage of the total surface area of a spacecraft's structure but have a significant influence on the overall spacecraft probability of penetration by M/OD impacts. Previous studies of impacts into glass using aluminum and glass projectiles have been documented [5-10]. This study differs from previous work on windows in that a wide range of projectile types were used in the tests, and an effort to characterize internal damage to fused silica glass was made by sectioning the targets and examining the internal damage from the side. The HITF conducted a systematic test program to determine impact characteristics and refine damage equations of fused silica, polycarbonate and tempered glass.

2. HVI Test Facilities

The HITF conducted the tests using a 4.3mm bore diameter, two-stage light-gas gun launcher at the White Sands Test Facility in Las Cruces, New Mexico. Testing was performed at ambient temperature and below 0.05 psia (2.6 mm Hg) chamber pressure. Impact velocity and projectile integrity were measured by means of a Cordin high-speed shadowgraph camera and laser intervalometers. A "good" test occurs when projectile velocity is obtained by two or more independent means, projectile integrity¹ is verified after launch but prior to impact, and the shot is "clean" with no major damage to the target other than from the projectile.

3. Fused Silica (SiO₂) Impact Testing

Fused silica is a high purity synthetic amorphous silicon-dioxide produced by flame hydrolysis. The Space Shuttle program has been using HPFS² fused silica for the Orbiter vehicle windows because of the materials low coefficient of thermal expansion and exceptional optical quality. Each of the four Orbiters has a total of 8 central windows in pairs (port and starboard) forward, middle, side, and overhead positions. Each of these windows comprises an outer thermal pane, a middle redundant pressure pane, and an inner redundant pressure pane. The HITF conducted HVI testing on orbiter windows using a variety of projectile materials (aluminum, steel, nylon, brass, and sapphire) to provide detailed comparison data for more accurate post-flight inspections and refining damage characteristics and equations.

3.1 SiO₂ Test Article and Test Matrix

Test articles consist of a fused silica target and an aluminum witness plate. The fused silica material used in this test program was taken from post-flight orbiter thermal pane windows. As part of NASA's effort to characterize and evaluate the M/OD environment in low Earth orbit, Space Shuttle Orbiter Fused Silica windows are inspected for hypervelocity impact damage after each flight. Measurements, mold impressions, and core samples are taken from impacted areas to access the particle parameters (size, velocity, angle, and density) and determine if the impactor was a naturally occurring meteoroid or man-made orbital debris. Over 130 windows have been replaced due to impact damage, and some of these previously flown windows were made available for the HVI testing reported here.

A 76 mm diameter samples were taken from non-damaged³ sections of the orbiter panes. Samples were mounted in a circular flange support fixture and surrounded by Buna-80 soft gasket material. A 1 mm thick Al 2024-T3 witness plate is located 76 mm behind the fused silica. Test article configuration is illustrated in Figure 1.

¹ Intact projectile with constant shape.

² HPFS is a trademark of Corning, Inc.

³ Areas without prior impact damage or residue.

Twenty-five tests were conducted using 0.4 mm diameter Al2017-T4 spherical projectiles with impact velocities varying from 7 km/s to 2.5 km/s in 0.5 km/s increments. The impact angles were 0° and 45° for each velocity with some additional tests conducted at 30° and 60°. Additional tests were performed with larger aluminum projectiles, as well as steel, nylon, aluminum-oxide and copper alloy projectiles at various impact velocities and angles.

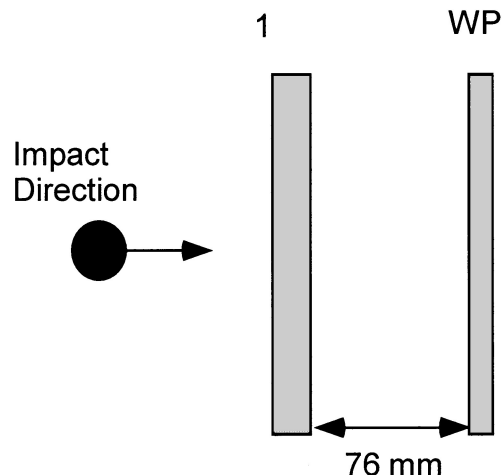
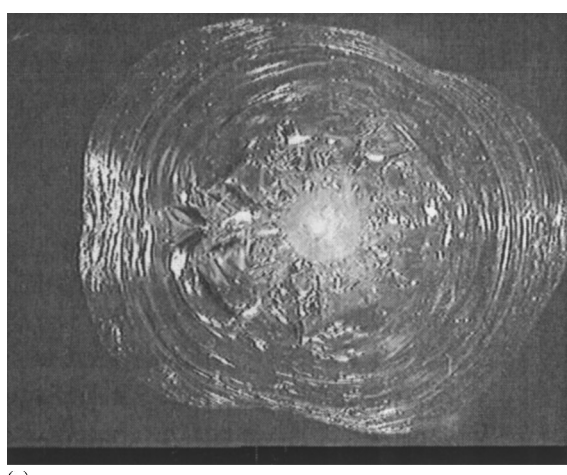


Fig. 1. Test article configuration.

3.2 High Velocity Damage Characteristics

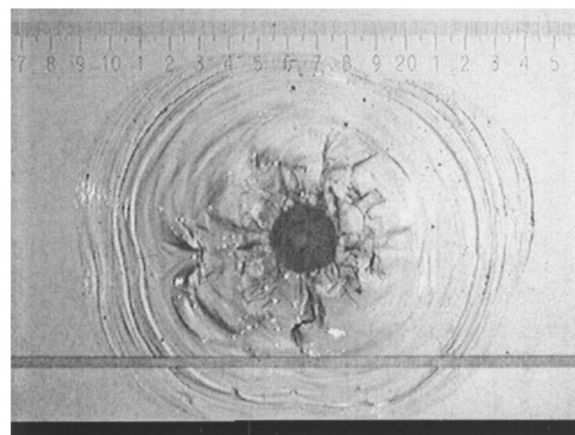
High velocity damage in fused silica results in front-side craters with large diameter relative to crater depth (Figures 2a and 2b), and internal flaws. Impact crater shapes typically become more elliptical with increases in the impact angle (Figures 3 and 4). Impact craters have circular pattern contours in the outer regions and a center area of heavier damage that appears white. HVI targets had straight, parallel sides cut and polished several centimeters away from the impact damage. The polished sides provided a window to examine internal crack morphology. An example of the internal cracks from the impact damage shown in Figure 2 is provided in Figures 4a – 4c. For this particular impact, cracks were measured 0.4mm in length below the crater (0.9mm deep crater, cracks and crater 1.3mm deep).



(a)

Fig. 2a. Impact Crater from JSC-120069 (front-lit view).

Crater: 15.8mm diameter by 0.9mm deep
Projectile: 0.4mm diameter Al, 5.24km/s, 0°.



(b)

Fig. 2b. Impact Crater from JSC-120069 (back-lit view).

Crater: 15.8mm diameter by 0.9mm deep
Projectile: 0.4mm diameter Al, 5.24km/s, 0°.

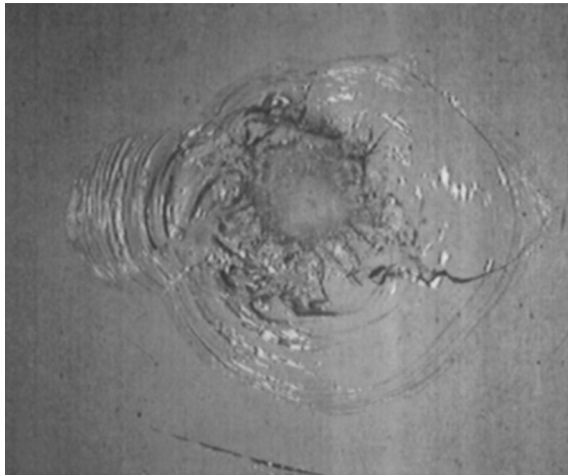


Fig. 3. Impact Crater from JSC-120066.
Projectile: 0.4mm diameter Al, 5.1km/s, 45°.

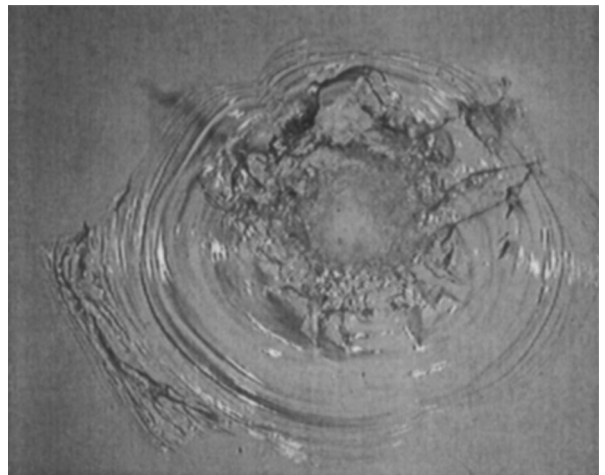


Fig. 4. Impact Crater from JSC-120068.
Projectile: 0.4mm diameter Al, 6.29km/s, 45°.

Measurements of crack morphology are continuing for several HVI tests into fused-silica glass. The length and shape of the cracks and surface craters will be used in structural analysis codes to assess residual strength of the glass. The damaged glass will also be subjected to bending tests to determine residual strength, with the data used to calibrate and verify the predictive tools.

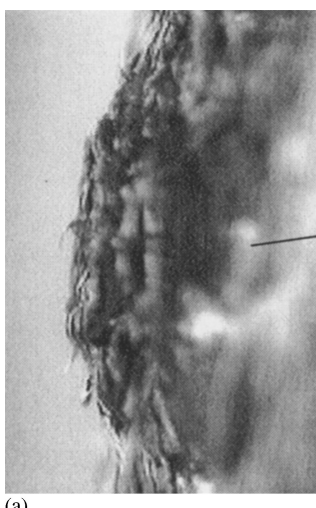


Fig. 4a. Close-up of internal flaws directly below impact point JSC-120069.

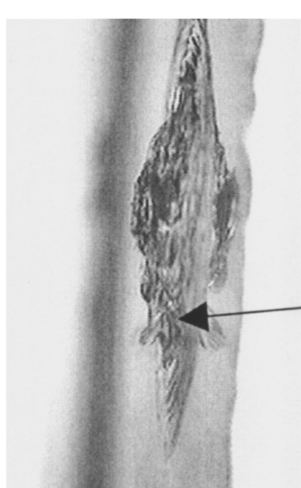


Fig. 4b. Internal view of impact crater (side view)
JSC-120069.



Fig. 4c. Close-up of internal flaw in spall zone
of crater (side view)
JSC-120069.

3.3 Internal Glass Damage Due to Edge Effects

Sample size and edge mounting conditions are important in the glass HVI testing. Rubber gaskets to eliminate metal-to-glass contact during the tests were used to protect the edge of the glass samples. Otherwise shock waves and vibrations could splinter and crack the glass edges and could propagate to the entire sample.

Small glass samples are desirable to conserve expensive target material. However, small samples can result in edge effects that influence the extent of damage to the target. Due to its brittle nature and low tensile strength, glass is subject to more damage from edge effects if sample size is too small. Edge effect damage is characterized by internal damage on the back and sometimes front of the glass that does not correspond directly to the impact point. This is most evident when impacts are not centered on the target. Edge effect damage is caused by the intersection of tensile waves after reflection of the initial compressive shock waves off the edges of the sample as illustrated in Figure 5. The interaction of the tensile waves is strongest at the anti-nodal position from the impact point, which is on opposite side from the center of circular target as the impact point, and is concentrated at a distance from the center of

a circular target that is the same distance (but in opposite direction) as the projectile impact point from the center of a circular target. An example of the phenomena is illustrated in Figure 6, which shows a heavy concentration of internal cracking near the bottom surface of a glass target at an anti-nodal point from the impact crater. The location of the phenomena is symmetric with the impact crater about the center of the target confirming that it is an edge effect of the target configuration.

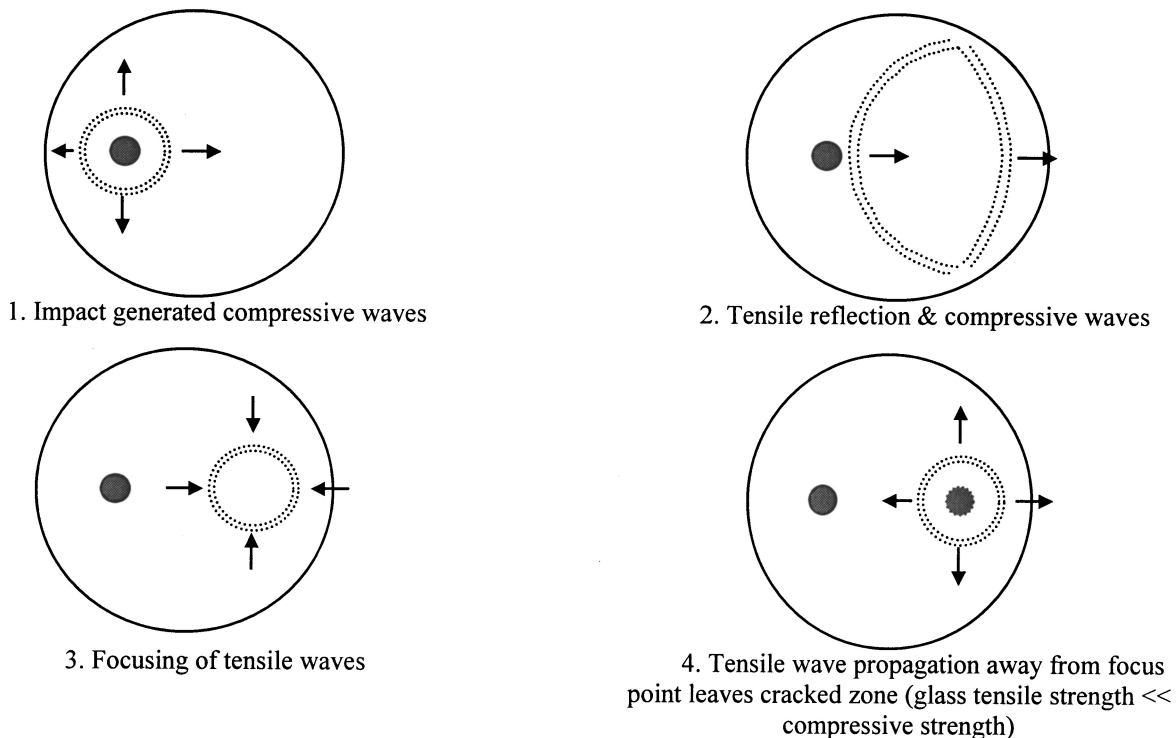


Fig. 5. Edge effect phenomenon illustration.

Edge effects are sample size dependent, occurring more commonly as target size decreases. Also, it depends on impact characteristics, with higher impact shocks more likely to cause an edge effect. Typically, glass samples 8cm in diameter would be subject to edge effect damage if impacted by 0.4mm diameter aluminum projectiles at 6.8km/s, normal impact. However, it takes a 0.8mm diameter aluminum projectile at 6.8km/s, normal impact to generate edge effects in fused silica glass samples 22.5cm in diameter.

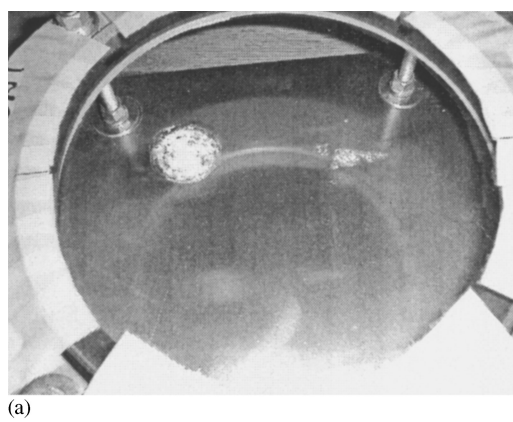


Fig. 6a. Impact crater on left and edge effect internal crack damage on right. Projectile: 0.8mm diameter Al, 6.9km/s, 0° JSC-HITF02199.

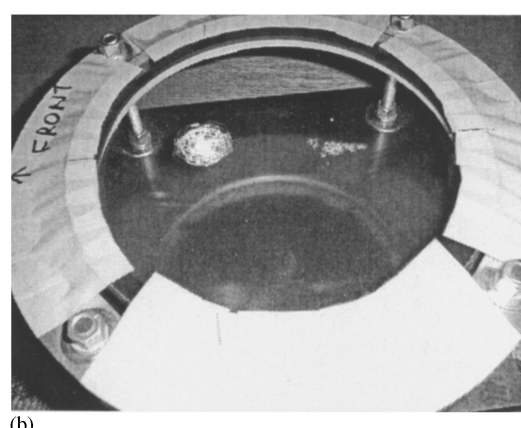


Fig. 6b. Target: 22.5cm diameter by 1.5cm thick fused silica glass JSC-HITF02199

Edge effects will not be evident in impacts that are centered on circular targets because the edge effect damage will lie right on-top the damage from the projectile, and be indistinguishable from the primary impact damage. However, edge effects will increase the apparent target damage. It is an

important consideration when conducting and comparing damage to circular glass or brittle (ceramic) targets in any HVI test series.

Changes to the target edges of circular targets will reduce the potential for edge effect damage. Notching the edges of circular targets, or scalloping the edge will eliminate/reduce the focusing of reflected shock waves and thereby decrease edge effect damage as shown in Figure 7. Also, of course, non-circular glass targets will also be far less sensitive to this problem.

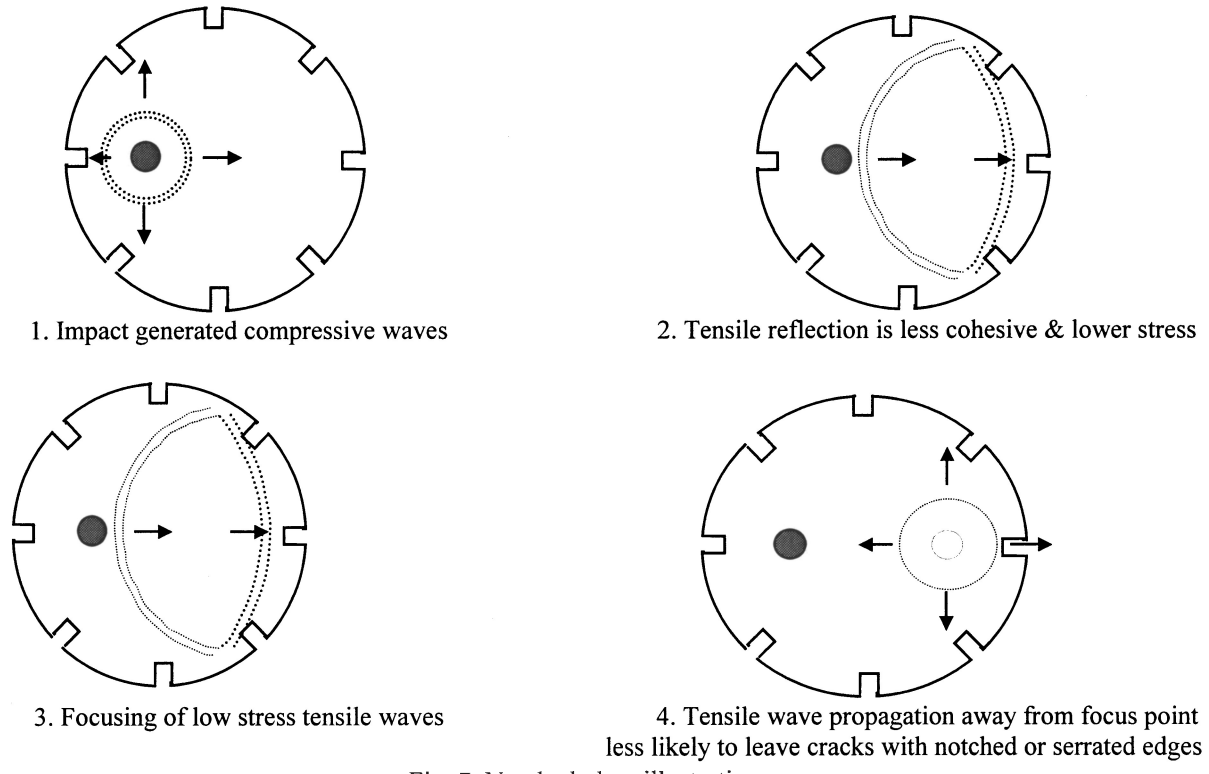


Fig. 7. Notched glass illustration.

There are many viewports and windows on spacecraft that are circular in shape. Based on this HVI test data, it is suggested that the edges of fused-silica glass in circular spacecraft windows be roughened or notched to reduce the potential for edge effect damage.

3.4 Low Velocity Damage Characteristics

Low velocity damage characteristics include smaller and shallower front side surface spallation zones (Figure 8). Impact crater shapes typically become more circular at oblique impact angles as the velocity decreases. Impact craters have circular pattern contours in the outer regions and a center area of heavy damage that appears white. Edge effects are not as pronounced or apparent as velocity decreases.

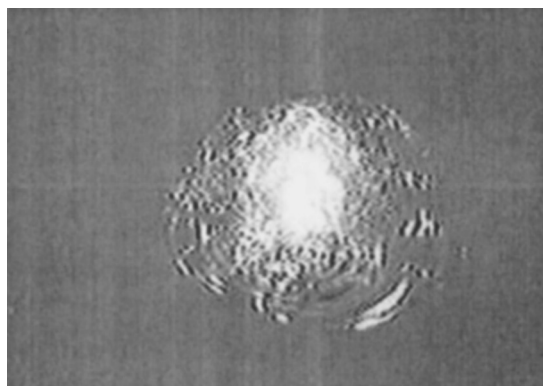


Fig. 8. Low velocity damage characteristics.

3.5 Damage Equations

Damage equations for fused silica previously developed from hypervelocity impact testing are given below:

Impact Crater Depth (Cour-Palais) [5-6]:

$$P = 0.53 \rho_p^{0.5} d_p^{1.06} V_N^{2/3} \quad (1)$$

Front Surface Crater (Spall) Diameter (Edelstein) [10]:

$$D = 30.9 \rho_p^{0.44} d_p^{1.33} V_N^{0.44} \quad (2)$$

Where P is the crater depth (cm), D is the front side crater (spall) diameter (cm), ρ_p is the projectile density (g/cm^3), d_p is the projectile diameter (cm), and V_N is the normal component of the projectile velocity (km/s).

The damage equations were modified using the new test data to better model the actual impact damage. The modified equations are given below:

Modified Impact Crater Depth:

$$P = 0.266 \rho_p^{0.595} d_p^{1.05} V^{0.995} \cos\Theta^{0.496} \quad (3)$$

Modified Front Surface Crater Diameter:

$$D = 9.656 \rho_p^{0.373} d_p^{1.183} V^{0.915} \cos\Theta^{0.545} \quad (4)$$

A comparison of the predicted impact crater depths using both equations to the measured test data is given below in Figure 9. A similar comparison of the predicted front surface spall diameter using both equations to the measured test data is given in Figure 10. The equations were derived from regression analysis, but do not provide substantially more accurate predictions than the old equations. It is recommended that additional higher velocity ($>7\text{ km/s}$) and more oblique impact angle tests be conducted to examine correlation from higher impact speeds and obliquity effects.

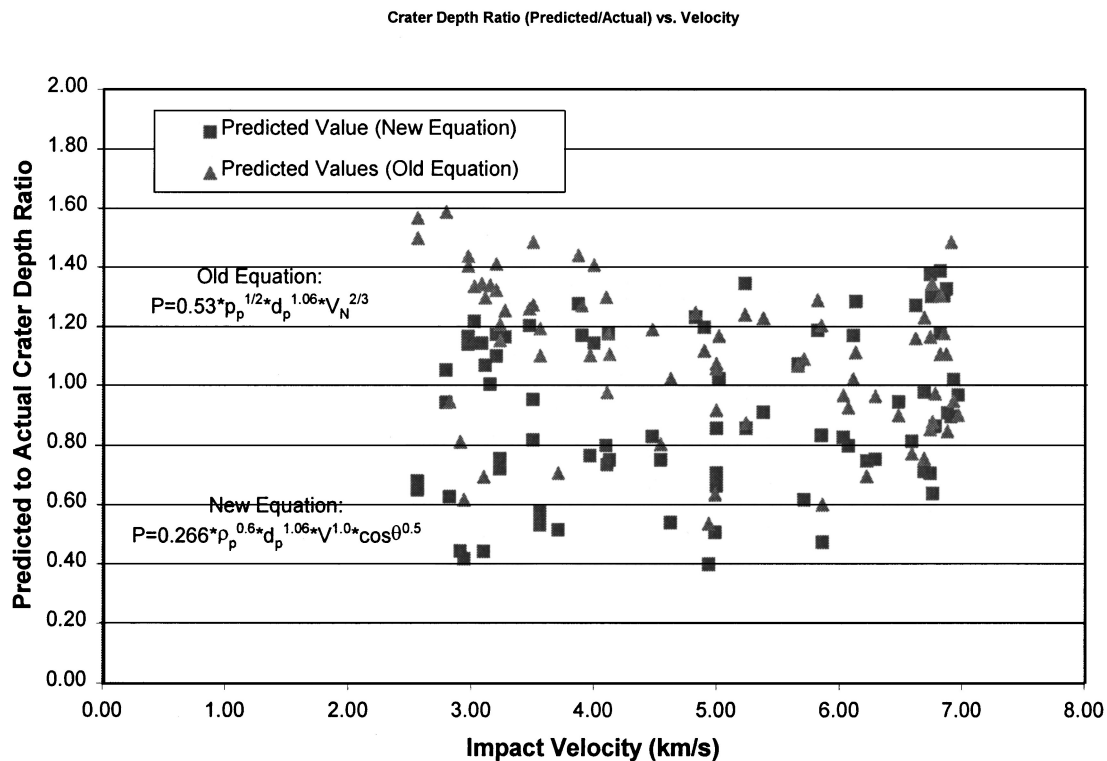


Fig. 9. Predicted crater depths comparison.

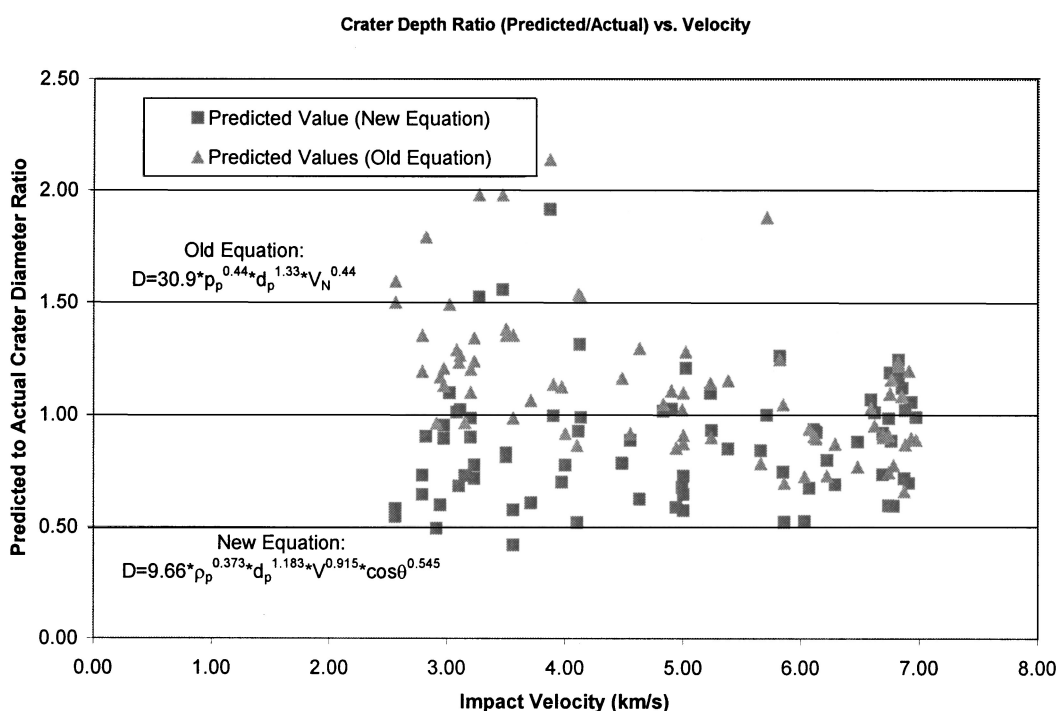


Fig. 10. Predicted crater diameter comparison.

4. Tempered Glass (Chemcor)

The Space Station Unity module or Node 1 was launched on STS-88 in December 1998 and provides docking ports for attachment of up to six other modules. Node 1 measures 5.5 meters long and

4.6 meters in diameter and it will provide connecting points for various ISS elements. The Node 1 Nadir hatch, shown in Figure 11, has a 25cm diameter window in the center made of two panes of Chemcor glass shielded by a MM/OD soft cover made of beta-cloth and Kevlar fabric, with a “flap” that can be opened to allow the crew and instrumentation to look through the hatch window during berthing operations for station elements that mate to the nadir docking port.

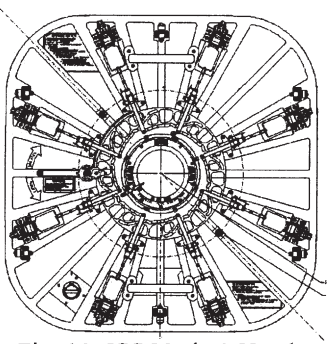


Fig. 11. ISS Node 1 Hatch with center CHEMCOR window.

the combination of compression and tension layers represent stored “energy” that is contained in each tempered glass layer.

A hatch window pane, shown in Figure 12, is made of two 4 mm thick Chemcor plies with a 1.8 mm thick Silicone interlayer. For the hatch window, compression layers are an average of 0.2 mm thick while tension layers are an average of 3.7 mm thick.

⁴ Chemcor is a trademark of Corning, Inc.

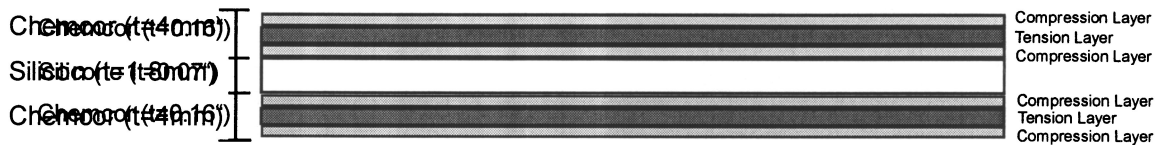


Fig. 12. Chemcor laminate window pane composition.

For HVI testing purposes, Modulus of Rupture (MOR) bars from the flight hardware scratch panes were used to represent hatch panes in the test articles. MOR bars are made with sets of tempered material to test the bending strength of the stock. The scratch pane MOR bars used for testing are 0.7 mm thicker than the hatch window.

The impact failure mode for Chemcor glass is a flaw deeper than the compression layer that causes the release of the stored temper energy and the pane to shatter. At low velocity impacts, below the hypervelocity regime, larger impactor energy is required to create a flaw in Chemcor glass than in an annealed Fused Silica. Preliminary estimate of the ballistic limit were based on the size aluminum projectile necessary to create a 0.2 mm crater in annealed fused silica. A 0.08 mm diameter aluminum projectile normally impacting at 6.8 km/s was estimated to have the required kinetic energy.

Due to limitation of the HITF two-stage light gas gun, the smallest particle that can be tested is 0.4 mm diameter. Both normal and oblique impact tests were completed.

One test was conducted with a 0.4 mm diameter Al2017-T4 spherical projectile normally impacted (0°) at 6.89 km/s. The test article consisted of two 3.8 cm by 25.6 cm MOR bars (1 and 2) separated by 1.8mm gap of air and followed 101 mm behind by a aluminum witness plate as seen in Figure 13.

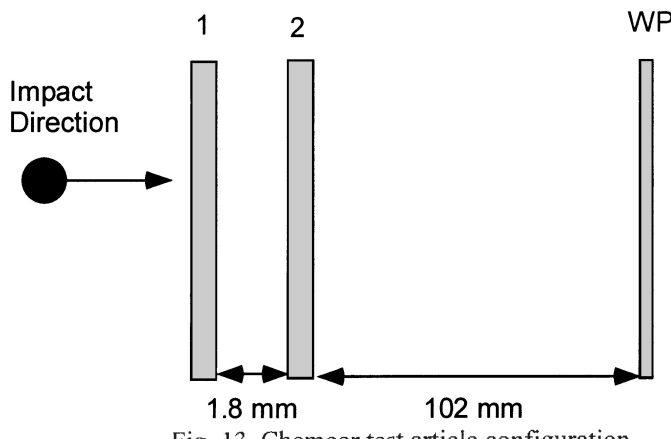


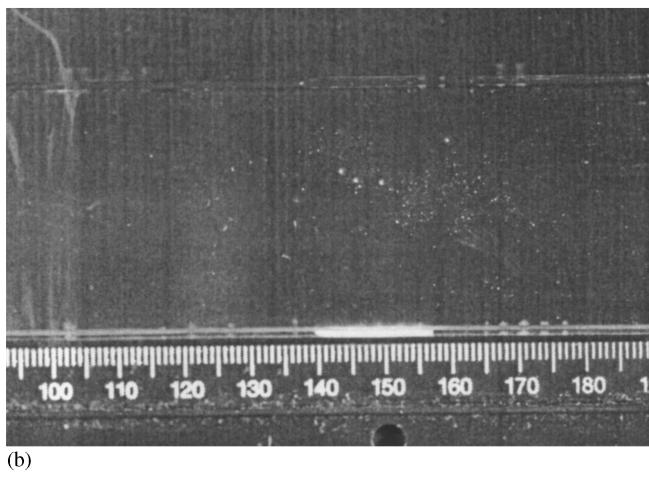
Fig. 13. Chemcor test article configuration.

This test resulted in complete failure of the first Chemcor pane with the largest remaining fragment measuring 3cm by 1.8cm shown in Figure 14a. Many thousands of smaller fragments were generated. The second Chemcor pane had some light surface debris but was not fractured and is shown in Figure 14b. A very similar result occurred with an impact by 0.4mm diameter aluminum projectile at 6.8 km/s and 45° impact angle.



(a)

Fig. 14a. 1st Pane Fragments (largest recovered).



(b)

Fig. 14b. 2nd Chemcor Pane.

5. Hyzod-AR Polycarbonate

Hyzod AR⁵ polycarbonate is a transparent amorphous thermoplastic with a hard coated surface that resists abrasion providing high impact strength and high modulus of elasticity. HYZOD AR has impact strength 250 times stronger than float glass and 30 times stronger than acrylic.

A 0.95cm thick Hyzod plate is used to protect the Node 1 hatch windows from M/OD impacts. Placement of the ISS Centerline Berthing Camera System in the Node 1 hatch window required an opening in the hatch debris soft-cover shield. Placement of Hyzod material as a transparent cover over the hatch window provides protection from direct meteoroid/orbital debris impact on the Chemcor glass used in the hatch window. The Hyzod cover is located approximately 66 mm from the exterior window pane. The cover is simply a 9.5 mm thick sheet of Hyzod AR hard-coated polycarbonate.

The purpose of this test program was to develop ballistic limit equations and damage characteristics for Hyzod material. The test matrix and results are shown below in Table 1.

Table 1. Test matrix and results

Test #	Projectile Diameter (mm)	Impact Angle	Actual Velocity (km/s)	Results	Penetration Depth (mm)	Back of Plate	Witness Plate
1	1.00	0°	7.09	Pass	0.68	No deformation	Clean
2	1.25	0°	6.56	Pass	0.81	Bulge: 0.05mm high	Clean
3	1.42	0°	6.89	Pass	1.08	Bulge: 0.24mm high	Clean
4	1.59	0°	6.72	Pass	2.59	Bulge: 0.67mm high	Clean
5	2.01	0°	6.64	Fail	7.8	Detached Spall: 3.9mm diameter	Deposits on surface (5cm diameter)
6	1.80	0°	6.81	Pass	6.43	Bulge: 2mm high	Clean
7	2.19	45°	6.78	Pass	4.46	Bulge: 2.5mm high; incipient detached spall: crack around 270° circumference of bulge	Clean
8	2.99	45°	4.02	Pass	5.6	Bulge: 2.5mm high; incipient detached spall: crack around 180° circumference of bulge	Clean

⁵ Hyzod AR is a trademark of Sheffield Plastics, Inc.

Ballistic limit equations (BLEs) are needed to assess meteoroid/debris failure probabilities in the BUMPER code. BLEs for the Hyzod have been developed from the hypervelocity test data given in this paper. These equations are based on the failure criterion of no damage to the witness plate; i.e., no damage to the Chemcor hatch window glass behind the Hyzod cover (Eq. 5-6). These equations are valid for 9.5mm thick Hyzod. Figure 15 shows the hypervelocity data plotted against the predictions using the ballistic limit equations (Eq. 5-6). Projectiles with normal component kinetic energy above the ballistic limit value of 185J will fail the Hyzod cover.

$$d_c = 0.1563 KE_{\text{limit}}^{1/3} V_n^{-2/3} \rho_p^{-1/3} \quad (5)$$

Where, d_c is the critical projectile diameter (cm) that results in threshold failure of the hyzod panel, V_n is the normal component of the projectile velocity (km/s); i.e., $V_n = V \cos\theta$, where θ is the impact angle measured from the target normal ($\theta=0^\circ$ is straight into the target), ρ_p is the projectile density (g/cm³), and

$$KE_{\text{limit}} = KE_f = 185J \quad (6)$$

KE_f is the critical projectile kinetic energy value (normal component) above which the 9.5mm thick Hyzod panel will be perforated or have detached spall on the back side of the Hyzod, which will result in damage to the witness plate behind the Hyzod.

Note, the units on the coefficient in Eq. (5) are $\{J^{-1/3} (\text{km/s})^{2/3} \text{ g}^{1/3}\}$.

5.1 No Spall Ballistic Limit for Hyzod

There will be no back-side spall effects of any kind on the Hyzod panel (9.5mm thick) when the projectile kinetic energy (normal component) is limited to the value given in Eq. (7). Projectile impacts with normal component kinetic energy above KE_{spall} will result in at least spall (a bump) on the back side of the Hyzod.

$$KE_{\text{limit}} = KE_{\text{spall}} = 37J \quad (7)$$

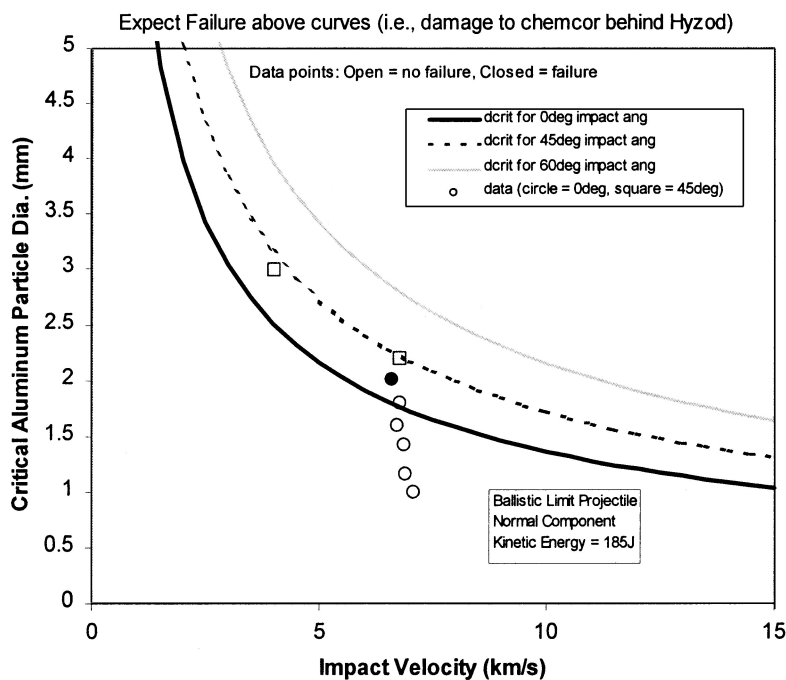


Fig. 15. Ballistic limits for a 9.5mm thick Hyzod Panel.

5.2 Penetration Equations for Predicting Depth of Penetration in Hyzod

Crater depth in Hyzod polycarbonate when penetration depths exceed 0.1cm is given in Eq.(8).

When $P > 0.1\text{cm}$,

$$P = 3.0 d_p^{1.2} V^{2/3} \cos^{0.75} \theta \rho_p^{1/3} - 1.38 \quad (8)$$

Where,

P is the crater depth (penetration depth) in the Hyzod (cm), d_p is the projectile diameter (cm), V is the projectile velocity (km/s), θ is the impact angle measured from the target normal ($\theta=0^\circ$ is straight into the target), and ρ_p is the projectile density (g/cm³).

Figure 16 shows the hypervelocity data plotted against the prediction of crater depth using Eq. (8).

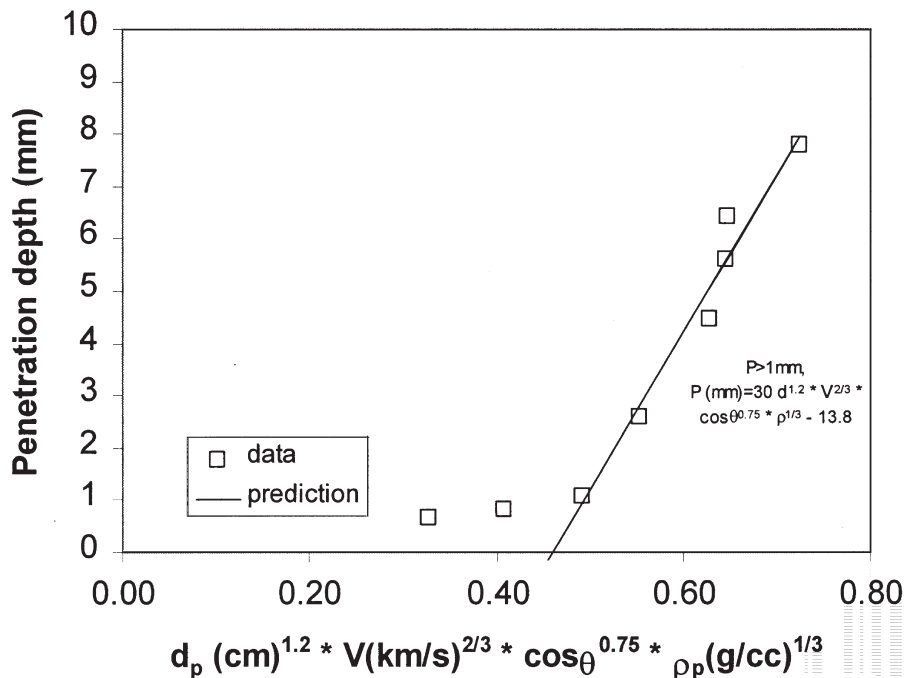


Fig. 16. Hyzod hypervelocity impact penetration depth.

5.3 Generalized Ballistic Limit Equations for Hyzod Panels of Variable Thickness

Preliminary equations have been developed for predicting failure limits for Hyzod as a function of Hyzod panel thickness. These equations are useful for assessing other Hyzod panel configurations.

The projectile energy parameter, ke_p (J^{1/3}), is defined as:

$$ke_p = KE_n^{1/3} / \cos^{1/3} \theta \quad (9)$$

Where KE_n is the normal component kinetic energy of the projectile (J), and θ is the impact angle measured from the target normal (deg).

Perforation of the Hyzod panel of thickness, t (mm), is predicted when:

$$t/ke_p \leq 1.5 \quad (10)$$

Detached spall from the back of the Hyzod panel of thickness, t (mm), is predicted when:

$$1.5 < t/ke_p \leq 1.6 \quad (11)$$

Attached spall (a bump) on the back of the Hyzod panel of thickness, t (mm), is predicted when:

$$1.6 < t/ke_p \leq 2.4 \quad (12)$$

6. Conclusions

A comparison of the Hyzod and Fused Silica mass per unit area to prevent perforation given the same impact conditions is shown in Figure 17. This figure illustrates the distinct difference in performance between various transparent materials. Hyzod polycarbonate exhibited significantly improved penetration performance when compared to Fused Silica of the same mass per unit area. Chemcor glass showed the least hypervelocity impact performance when compared with the other two materials. Currently, the HITF is working to characterize the M/OD penetration resistance of alternative transparent materials such as ceramic glass.

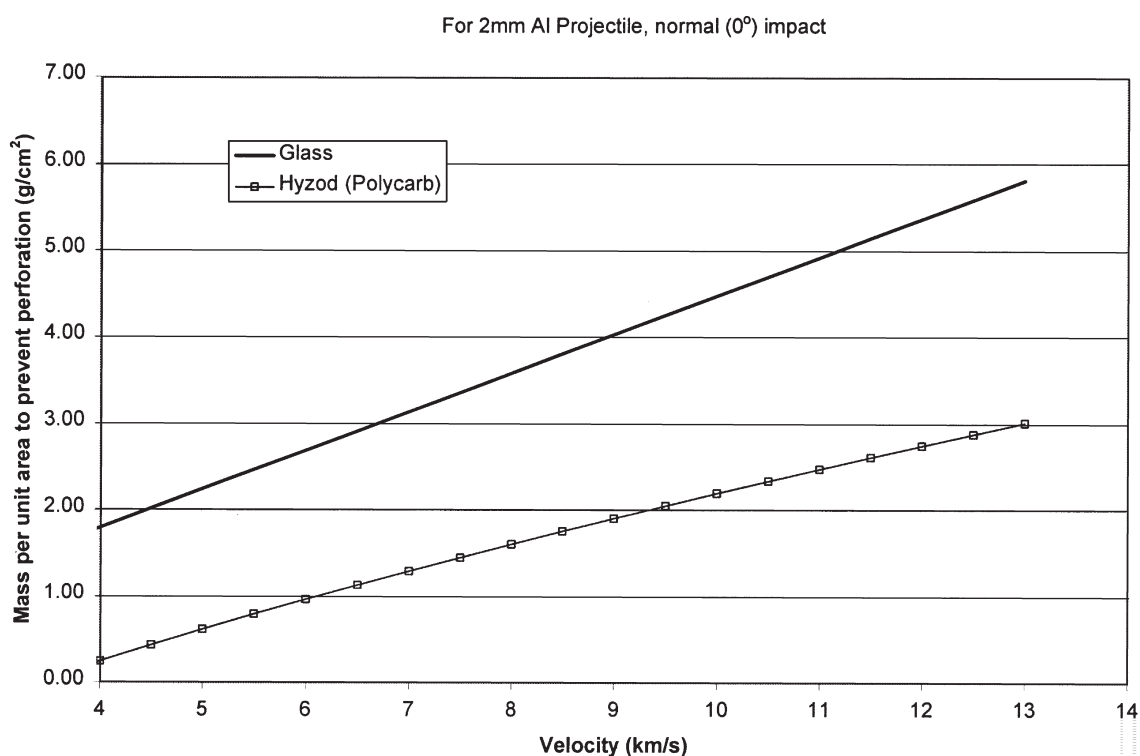


Fig. 17. Hyzod and Fused Silica mass per unit area to prevent perforation, 0.2cm diameter aluminum projectile impacts at 0°.

Acknowledgment

The authors thank the ISS Structures Manager, NASA JSC Kornel Nagy, and Lynda Estes/JSC-ES, for their assistance on this project. They also recognize contributions from JSC HITF personnel including Dana Lear, Tom Prior, Ron Bernhard, Frankel Lyons, Freeman Bertrand, Jay Laughman, Bill Davidson, Bobby Simpson, and Alan Davis; and WSTF personnel including Radel Bunker and Don Henderson.

References

- [1] Crews JL, Christiansen EL. The NASA JSC Hypervelocity Impact Test Facility (HITF), AIAA 92-1640, 1992.
- [2] NASA Johnson Space Center (JSC) Hypervelocity Impact Technology Facility (HITF) Web Site: <http://hitf.jsc.nasa.gov/hitfpub/main/index.html>
- [3] Christiansen EL. Design Practices for Spacecraft Meteoroid/Debris (M/D) Protection, Hypervelocity Shielding Workshop Proceedings, Institute of Advanced Technology (IAT), The University of Texas, Austin Texas, IAT Catalog Number IAT.MG-0004 (1999).
- [4] Christiansen EL, Kerr JH. Ballistic limit equations for spacecraft shielding, *Int. J. Impact Engng*, 2001, 26, 93-104.
- [5] Cour-Palais BG. A career in applied physics: apollo through space station, *Int. J. Impact Engng*, 1999, 23, 137-168.
- [6] Cour-Palais BG. Hypervelocity impact in metals, glass and composites, *Int. J. Impact Engng*, 1999, 5, 221-238.

- [7] Schneider E, Stilp AJ, Kagerbauer G. Meteoroid/debris simulation experiments on Mir viewport samples, *Int. J. Impact Engng*, 1995, **17**, 731-737.
- [8] Alwes D. Columbus viewport glass pane hypervelocity impact testing and analysis, *Int. J. Impact Engng*, 1990, **10**, 1-22.
- [9] Flaherty RE. Impact characteristics in fused silica, AIAA paper number 69-367 (1969).
- [10] Edelstein KS. Hypervelocity impact damage tolerance of fused silica glass, 43rd International Astronautical Federation, IAF-92-0334 (1992).
- [11] Burt R and Christiansen EL. Pre-Declared HVI Testing of ISS Hatch Window (Chemcor), NASA Report No. JSC-29421, August 2001.